



Full Length Article

An *in vitro* and *in silico* antidiabetic approach of GC–MS detected friedelin of *Bridelia retusa*

Somendra Kumar^a, Dinesh Kumar^a, Motiram Sahu^a, Neha Shree Maurya^b, Ashutosh Mani^b, Chandramohan Govindasamy^c, Anil Kumar^{a,*}

^a Department of Biotechnology, Govt. V.Y.T. PG. Auto. College, Durg, India

^b Department of Biotechnology, Motilal Nehru National Institute of Technology- Allahabad, India

^c Department of Community Health Services, College of Applied Medical Sciences, King Saud University, Riyadh, Saudi Arabia



ARTICLE INFO

Keywords:

Bridelia retusa
Antioxidants
Antidiabetic
GC–MS
Molecular docking

ABSTRACT

Bridelia retusa is a medicinal plant widely used to treat diabetes by ethnic populations worldwide, has been subjected to GC–MS-based profiling for the bark and fruit and identified 96 phytochemicals using ethyl acetate and methanol solvents. The DPPH antioxidant assay recorded that methanolic fruit extract had a maximum antioxidant activity of 83.01 % (IC₅₀-103.03 µg/ml). The α-amylase inhibition activity was found maximum in ethyl acetate bark extract with 76.34 % (127.37 µg/ml), while methanolic fruit extract exhibited the highest α-glucosidase inhibition activity with 86.18 % (106.15 µg/ml). Subsequently, we have compared the antidiabetic potential for 3 pharmacologically significant bioactive constituents friedelin, imidazole & sylvestrene through docking and drug likeliness study and found friedelin has a maximum binding affinity with different protein targets followed by sylvestrene and is most suitable candidate for drug development for hyperglycemia. Molecular dynamics simulations revealed friedelin as the most stable binder to anti-diabetic target proteins, with notable structural insights provided by RMSD, RMSF, SASA, and PCA analyses. MM-PBSA calculations emphasized the significance of various energies with the α-amylase-Friedelin complex exhibiting the highest binding energy.

1. Introduction

Medicinal plants contain abundant bioactive compounds with therapeutic potential. Although many phytoconstituents are identified in nature, only a few are isolated and studied for their bioactivity. Comprehensive phytochemical screening is crucial for discovering and developing effective medicinal agents with well-defined profiles.

Traditional healers practice *B. retusa* to treat various ailments, including diabetes, jaundice, and infections (Tatiya et al., 2011; Ghawate et al., 2014; Nguemem et al., 2009; Rupali et al., 2016). Despite its traditional use, there is a lack of scientific validation regarding its free radical scavenging capacity, anti-hyperglycemic activity, and receptor binding. The pharmaceutical industry faces challenges with drug development due to poor pharmacokinetic properties and inadequate receptor interactions, leading to financial losses. Molecular docking approaches are now employed to explore plant-based molecules for drug design and testing, offering valuable insights into binding interactions between drug candidates and target proteins (Konappa et al., 2020;

Loza-Mejía et al., 2018; Lee and Kim, 2019).

Therefore, the present study aims at qualitative phytochemical analysis, antioxidative and anti-hyperglycaemic evaluation for *B. retusa*, along with, *in silico* validation of the potential bioactive phyto-compounds to examine antidiabetic (e.g., α-amylase, α-glucosidase & DPP-IV) potential.

2. Materials and methods

2.1. Identification, and authentication

The specimen was collected from Durg, Chhattisgarh, India, in April 2021 (Fig. S1) and authenticated as *B. retusa* (L.) A.Juss. by BSI, Allahabad, India. The voucher number I (B.S.I/C.R.C. 2020–21/200) was assigned and deposited at BSI, Allahabad.

* Corresponding author.

E-mail address: anilkumardurg1996@gmail.com (A. Kumar).

<https://doi.org/10.1016/j.jksus.2024.103411>

Received 9 June 2024; Received in revised form 17 August 2024; Accepted 23 August 2024

Available online 31 August 2024

1018-3647/© 2024 The Authors. Published by Elsevier B.V. on behalf of King Saud University. This is an open access article under the CC BY-NC-ND license (<http://creativecommons.org/licenses/by-nc-nd/4.0/>).

2.2. Extraction and phytochemical screening

The bark and fruit of *B. retusa* were cleaned, powdered, and extracted with methanol and ethyl acetate using a Soxhlet extractor at 50–80 °C for 5–10 h. The extracts were filtered and analyzed for bioactive compounds, confirming the presence of alkaloids, cardiac glycosides, flavonoids, saponins, tannins, steroids, and terpenoids.

2.3. Phytochemical analysis by GC–MS

The samples were dissolved in methanol and ethyl acetate and injected into a Shimadzu® GC–MS QP2010 with a SH-I-5Sil MS Capillary column (30 m x 0.25 mm x 0.25 µm) in splitless mode. The oven temperature was set at 45 °C for 2 min, increased to 140 °C at 5 °C/min, then raised to 280 °C and held for 10 min. The injection volume was 2 µL, with helium at 1 mL/min flow rate and 70 eV ionization. The run time was 9.10 to 52.0 min. Compounds were identified by matching mass fragmentation patterns with the NIST 14. L library (Mallard and Linstrom, 2008).

2.4. Antioxidant activity

The DPPH assay, following Karamian et al. (2014), was used to estimate the free radical scavenging ability of *B. retusa* extracts. Solutions of the extracts (25–250 µg/ml) were mixed with 0.004 % methanolic DPPH, and incubated in the dark at 36 °C for 30 min, and their absorbance was recorded at 517 nm. A blank solution with methanol and DPPH was used as a control, with ascorbic acid as a reference. The IC₅₀ was calculated from the calibration curve using the linear regression equation.

$$\%inhibition = \frac{A_{con} - A_{test}}{A_{con}} \times 100$$

where A con– absorption of the control,

A test- absorbance with samples of the extracts.

2.5. Antidiabetic activity

The α-amylase inhibition assay for *B. retusa* fruit and bark extracts were determined by using the 3,5-dinitro salicylic acid method, with acarbose as a control. Absorbance was measured at 540 nm. The α-glucosidase inhibition assay was measured followed by Eom et al., (2012), with IC₅₀ calculated, both using acarbose as a standard.

$$\%inhibition = (Abs_{control} - Abs_{sample}) / (Abs_{control}) \times 100$$

2.6. Molecular docking

Friedelin, imidazole, and sylvestrene were selected for antidiabetic profiling via molecular docking, based on GC–MS analysis and literature. Their 3D structures were retrieved from PubChem, converted to PDFs using Open Babel, and were used for docking studies with diabetes-related target proteins: DPP-IV (PDB: 4A5S), α-amylase (PDB: 5KEZ), and α-glucosidase (PDB: 1UOK). Protein-ligand interactions were analyzed using UCSF Chimera, with the best binding poses determined by the lowest binding free energy. Drug-likeness was evaluated using SWISSADME, adhering to Lipinski's rule of five (Daina and Zoete, 2016; Kurjogi et al., 2018).

2.7. Molecular dynamics (MD) simulation of protein-ligand complexes

Molecular dynamics (MD) simulation was performed to assess the time-dependent stability of friedelin, imidazole, and sylvestrene complexed with DPP-IV (PDB: 4A5S), α-amylase (PDB: 5KEZ), and α-glucosidase (PDB: 1UOK). Using GROMACS-2022 with the CHARMM36 force field, ligand topology files were generated via the

CGenFF server, and protein topology files through pdb2gmx. The complexes were energy-minimized and equilibrated, followed by a 100 ns MD run. Trajectories were analyzed for RMSD, RMSF, Rg, hydrogen bonds, SASA, and PCA, with the Free Energy Landscape (FEL) visualized in 2D and 3D (Hess et al., 1997; Van Der Spoel et al., 2005; Vanommeslaeghe et al., 2010; Huang and MacKerell, 2013).

2.8. ΔG_{Bind} calculations through MM-PBSA for protein–ligand complex

The binding-free energy (ΔG_{Bind}) of protein–ligand complexes (DPP-IV, α-amylase, α-glucosidase) with friedelin, imidazole, and sylvestrene were calculated using the MM-PBSA method in GROMACS. This analysis, based on trajectories from the last 10 ns of MD simulation, helps evaluation of interaction energy, conformational changes, and entropy's role in binding affinity (Van Der Spoel et al., 2005).

$$\Delta G_{Bind} = \Delta G_{Complex} - (\Delta G_{Receptor} + \Delta G_{Ligand})$$

where, ΔG_{bind} is the total free energy of the protein–ligand complex and ΔG_{Receptor} and ΔG_{Ligand} are the total free energies of the separated protein and ligand in a solvent, respectively.

2.9. Statistical analysis

The experiments were conducted in triplicate (n = 3), and the data were presented as the mean ± standard deviation. The IC₅₀ values were determined and calculated using linear regression analysis with the aid of Microsoft Excel 2016 software.

3. Results and discussion

3.1. Phytochemical screening

GC–MS analysis of *B. retusa* extracts identified 96 peaks, revealing 34 compounds in methanol fruit and 38 in ethyl acetate fruit extracts. Additionally, 12 compounds from methanolic bark and 29 from ethyl acetate bark were recorded. These phytochemicals, detailed in (Table S1 to S6 & Fig. S2–S5) underscore the plant's therapeutic significance.

Tatiya et al., (2017) identified friedelin, β-sitosterol, stigmasterol, and lupeol in *B. retusa* bark with applications for pain and arthritis. Chitosan flavonoid was noted for analgesic and anti-inflammatory effects. Adhav et al., (2002) reported isoflavone with antiviral properties, and Kumar and Jain (2014) confirmed β-sitosterol, ellagic acid, and gallic acid as antifungal, antibacterial, and antioxidant. Additional compounds such as bisabolene sesquiterpenes, various benzoic acids, and sesamin were identified by Jayasinghe et al., (2003) and Umar et al., (2022), with potential SARS-CoV-2 inhibition. Ogbonnia et al. (2021) described other compounds in *Bridelia ferruginea*. Present study provides a comprehensive description of 92 compounds from *B. retusa*, with 88 as newly reported.

3.2. Antioxidant activity

In the DPPH assay, the ability of the extracts to donate hydrogen atoms or electrons was assessed, leading to DPPH% reduction to DPPH-H. The IC₅₀ values were determined from calibration curves and compared to ascorbic acid. The methanolic fruit extract of *B. retusa* showed the highest DPPH scavenging activity at 83.01 % and an IC₅₀ of 103.03 µg/ml. It was followed by the ethyl acetate fruit extract (IC₅₀: 135.66 µg/ml), ethyl acetate bark extract (IC₅₀: 185.8 µg/ml), and methanolic bark extract (IC₅₀: 206.72 µg/ml). In a similar study, the scavenging activity was reported as follows: ascorbic acid > aqueous extract > ethanol extract > methanol extract > 50 % ethanol extract > 50 % methanol extract > 70 % acetone extract, with IC₅₀ values of 58.78 %, 62.61 %, 62.27 %, 61.94 %, 62.61 %, 70.46 %, and 61.93 %, respectively.

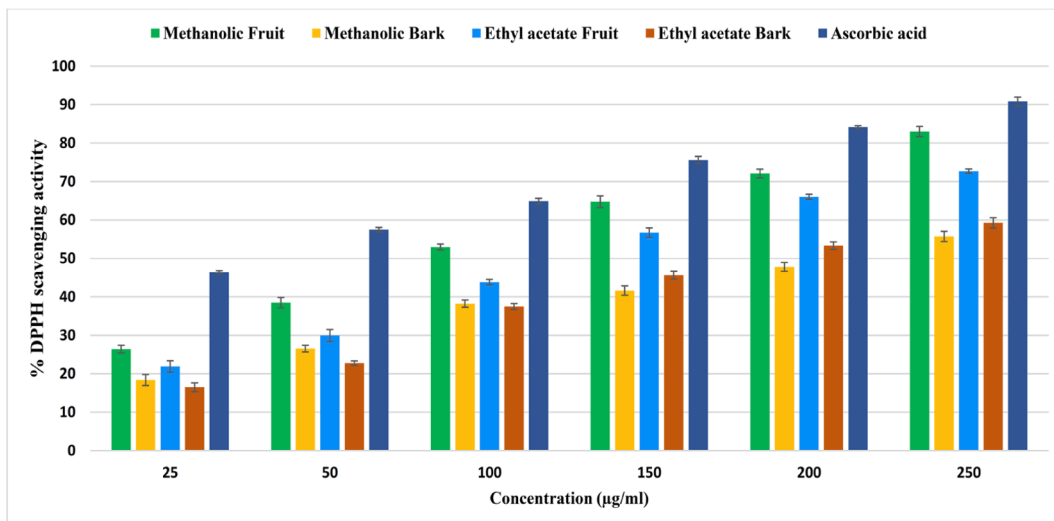
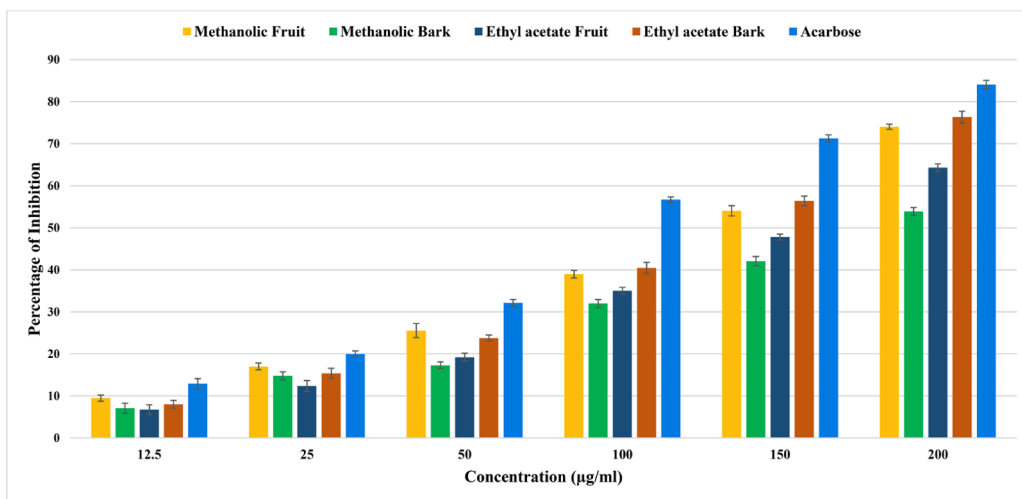
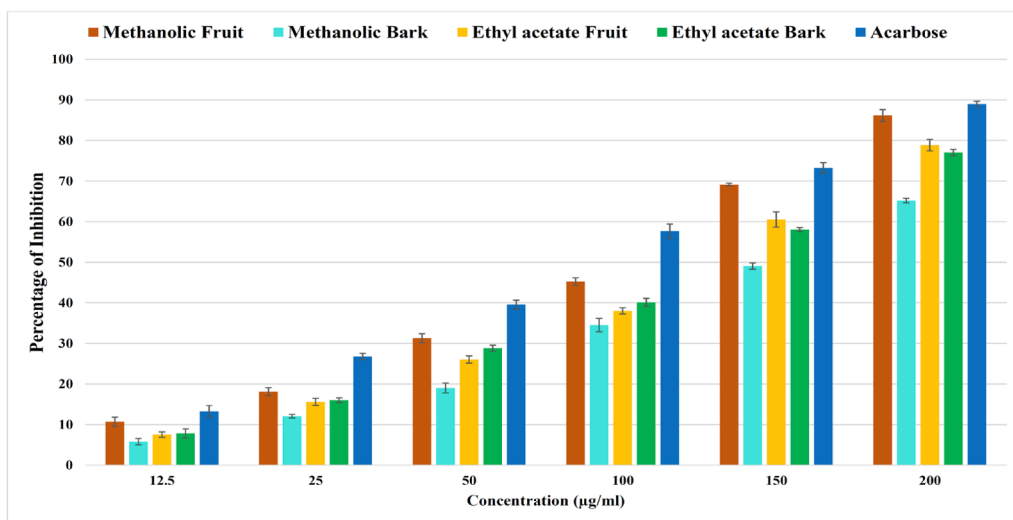


Fig. 1. showing antioxidant activity of *B. retusa* fruit and bark extract through DPPH radical scavenging activity.



a



b

Fig. 2. showing antidiabetic enzymes activities of *B. retusa* fruit and bark extracts. (a) α-amylase inhibition activity, (b) α-glucosidase inhibition activity.

Table 1Structures and retention time (min) of phytochemical constituents identified in methanol and ethyl acetate extract of *B. retusa* fruit and bark using gas chromatography-mass spectrometry.

S. No.	Retention time	Name of the compound	Structure
	RT-2.156	Furfural	C1=COC(=C1)C=O
	RT-3.050	Glycerin	C(C(CO)O)O
	RT-3.795	Pyrovalerone	CCCC(C(=O)C1 = CC=C(C=C1)C)N2CCCC2
	RT-4.339	Pyranone	C1=CC(=O)OC=C1
	RT-5.252	Hydroxymethylfurfural	C1=C(C(OC(=C1)C=O)CO
	RT-6.028	3-Octanol, 2,6-dimethyl-, acetate	CCC(C)CCC(C(C)C)OC(=O)C
	RT-6.785	1,4-Dioxane, 2-ethyl-5-methyl-	CCC1COC(CO1)C
	RT-7.091	Pyrogallol	C1=CC(=C(C(=C1)O)O)O
	RT-7.542	D-Allose	C([C@@H]1[C@H]([C@H]([C@H](C(O1)O)O)O)O)O
	RT-8.236	α -D-Galactopyranoside, methyl	O1[C@H](OC)[C@H](O)[C@@H](O)[C@H](O)[C@H]1CO
	RT-8.624	d-Mannose	C([C@@H]1[C@H]([C@@H]([C@H](C(O1)O)O)O)O)O
	RT-8.886	Tetradecanoic acid	CCCCCCCCCCCC(=O)O
	RT-9.331	3-O-Methyl-d-glucose	CO[C@H]([C@H](C=O)O)[C@@H]([C@@H](CO)O)O
	RT-10.425	Hexadecanoic acid, methyl ester	CCCCCCCCCCCCCCCC(=O)OC
	RT-10.782	Benzenepropanoic acid, 3,5-bis(1,1-dimethylethyl)-4-hydroxy-, methyl ester	CC(C)(C)C1=CC(=CC(=C1O)C(C)(C)C)CCC(=O)OC
	RT-11.120	n-Hexadecanoic acid	CCCCCCCCCCCCCCCC(=O)O
	RT-11.676	Isopropyl palmitate	CCCCCCCCCCCCCCCC(=O)OC(C)C
	RT-12.552	Heptanoic acid, 4-octyl ester	CCCCCCC(=O)OC(CCC)CCCC
	RT-12.796	9,12-Octadecadienoic acid, methyl ester	CCCCC/C=C\C/C=C\C\CCCCCCCC(=O)OC
	RT-12.877	Methyl petroselinatate	CCCCCCCCCCC/C=C\C\CCCC(=O)OC
	RT-13.121	Phytol	C([C@@H](CCCC[C@H](C)CCC/C(=C/CO)/C)CCCC(C)C
	RT-13.259	Heptadecanoic acid, 16-methyl-, methyl ester	CC(C)CCCCCCCCCCCCCCCC(=O)OC
	RT-13.897	Linoleic acid	CCCCC/C=C\C/C=C\C\CCCCCCCC(=O)O
	RT-14.166	Octadecanoic acid	CCCCCCCCCCCCCCCC(=O)O
	RT-17.913	Eicosanoic acid (Arachidic acid)	[2H]C([2H])([2H])CCCCCCCCCCCCCCCC(=O)O
	RT-19.902	Hexanoic acid, 2-ethyl-, hexadecyl ester	CCCCCCCCCCCCCCCCOC(=O)C(CC)CCCC
	RT-20.328	Hexadecanoic acid, 2-(octadecyloxy)ethyl ester	CCCCCCCCCCCCCCCCCOC(=O)CCCCCCCCCCCCCCCC
	RT-21.110	Hexadecanoic acid, 2-hydroxy-1-(hydroxymethyl)ethyl ester	CCCCCCCCCCCCCCCC(=O)OC(CO)CO
	RT-21.560	Diisooctyl phthalate	CC(C)CCCCOC(=O)C1 = CC=CC=C1C(=O)OCCCC(C)C
	RT-24.256	Hexanoic acid, 2-ethyl-, octadecyl ester	CCCCCCCCCCCCCCCCCOC(=O)C(CC)CCCC
	RT-26.839	Erucylamide	CCCCCCCC/C=C\C\CCCCCCCCCCCC(=O)N
	RT-27.503	Squalene	CC(=CCC/C(=C/C/CC/C(=C/C/CC/C=C/C/CCC=C(C)C)\C)/C)/C
	RT-31.362	Rhodopin	CC(=CCC/C(=C/C=C/C(=C/C=C/C/C=C/C=C(C\C)/C=C/C=C(C)/C=C/C=C(C)/C)/C)/C
	RT-32.926	Friedelin	C([C@H]1C(=O)CC[C@@H]2[C@@H]1(CC[C@H]3[C@H]2(CC[C@@H]4[C@@H]3(CC[C@@H]5[C@@H]4CC(C5)C)C)C)C)C
	RT-2.617	Ethyl Acetate	CCOC(=O)C
	RT-4.550	Propyl acetate	CCCOC(=O)C
	RT-11.238	<i>trans</i> -Chrysanthenyl acetate	CC1 = CC[C@H]2[C@H]([C@H]1C2(C)C)OC(=O)C
	RT-21.740	1-Undecanol	CCCCCCCCCCCCO
	RT-25.209	Dodecanoic acid, 10-methyl-, methyl ester	CCC(C)CCCCCCCC(=O)OC
	RT-27.898	Dioctyl terephthalate	CCCCCCCCOC(=O)C1 = CC=C(C=C1)C(=O)OCCCCCCCC
	RT-29.103	Dodecyl acrylate	CCCCCCCCCCCCOC(=O)C=C
	RT-34.731	Terephthalic acid, 4-octyl octyl ester	CCCCCCCCOC(=O)C1 = CC=C(C=C1)C(=O)OC(CCC)CCCC
	RT-37.234	Methyl octadeca-9,12-dienoate	CCCCC=C=CC=C(CCCCCCCCC(=O)OC
	RT-37.340	<i>trans</i> -13-Octadecenoic acid, methyl ester	CCCC/C=C/C\CCCCCCCCCCCC(=O)OC
	RT-37.804	Methyl stearate	CCCCCCCCCCCCCCCC(=O)OC
	RT-42.505	Hexanedioic acid, bis(2-ethylhexyl) ester	CCCC(C)COC(=O)CCCC(=O)OCC(C)CCCC
	RT-3.163	Tridecane	CCCCCCCCCCCCC
	RT-3.569	Octane, 5-ethyl-2-methyl-	CCCC(C)CCC(C)C
	RT-4.389	2-Dodecene, (Z)-	CCCCCCCC/C=C\C
	RT-5.146	Dodecane, 2,6,11-trimethyl-	CC(C)CCCC(C)CCCC(C)C
	RT-5.265	Pentadecane	CCCCCCCCCCCCC
	RT-5.327	Dodecane, 5,8-diethyl-	CCCC(C)CCC(C)CCCC
	RT-5.665	Undecane, 4,7-dimethyl-	CCCC(C)CCC(C)CCC
	RT-5.728	Hexane, 3,3-dimethyl-	CCCC(C)(C)CC
	RT-6.034	Cetene	CCCCCCCCCCCCCCC=C
	RT-6.766	Hexadecane	CCCCCCCCCCCCCCCC
	RT-7.060	Hexadecane, 2,6,11,15-tetramethyl-	CC(C)CCCC(C)CCCC(C)CCCC(C)C
	RT-7.129	Disulfide, di- <i>tert</i> -dodecyl	CCCCCCCC(C)(C)SSC(C)(C)CCCCCCCC
	RT-7.273	Heptadecane, 2,6,10,15-tetramethyl-	CC(C)CCCC(C)CCCC(C)CCCC(C)C
	RT-8.286	Eicosane, 2-methyl-	CCCCCCCCCCCCCCCC(C)C
	RT-8.549	Eutanol G	CCCCCCCC(C)CCCC(C)CO
	RT-8.799	Heptadecane, 3-methyl-	CCCCCCCC(C)CCCC(C)CC
	RT-8.861	2-Octadecoxyethanol	CCCCCCCCCCCCCCCCOCCO
	RT-8.905	Octadecanoic acid, 4-hydroxy-, methyl ester	CCCCCCCCCCCCCCCC(CCC(=O)OC)O
	RT-9.005	Hexadecen-1-ol, <i>trans</i> -9-	CCCCC/C=C/C\CCCCCCCCO
	RT-9.931	Cyclopropanoic acid, 2-[(2-pentylcyclopropyl)methyl]-, methyl ester, trans,trans-	CCCC[C@@H]1CC1CC2C[C@H]2CCCCCCCC(=O)OC

(continued on next page)

Table 1 (continued)

S. No.	Retention time	Name of the compound	Structure
RT-10.432		Hexadecanoic acid, methyl ester or Methyl palmitate	CCCCCCCCCCCCCCCC(=O)OC
RT-10.619		7,9-Di- <i>tert</i> -butyl-1-oxaspiro(4,5)deca-6,9-diene-2,8-dione	CC(C)(C)C1 = CC2(CCC(=O)O2)C=C(C1 = O)C(C)C(C)
RT-10.888		Eicosane, 7-hexyl-	CCCCCCCCCCCCCCCC(CCCCC)CCCCC
RT-11.245		2-Hexadecanol	CCCCCCCCCCCCCCCC(C)O
RT-12.546		Heptanoic acid, anhydride	CCCCCCC(=O)OC(=O)CCCCC
RT-12.796		8,11-Octadecadienoic acid, methyl ester	CCCCC/C=C/C/C=C/C/CCCCC(=O)OC
RT-12.877		10-Octadecenoic acid, methyl ester	CCCCCCC/C=C/C(CCCCCC(=O)OC)O
RT-13.365		Octadecane, 3-ethyl-5-(2-ethylbutyl)-	CCCCCCCCCCCCC(CC(CC)CC)CC(CC)CC
RT-14.347		10-Heneicosene (c,t)	CCCCCCCCC/C=C/CCCCCCCC
RT-18.201		Hexacosyl acetate	CCCCCCCCCCCCCCCCCCCCCCCCCCCC(=O)C
RT-29.091		Tetracontane	CCCCCCCCCCCCCCCCCCCCCCCCCCCCCCCC
RT-3.292		Isobutyl acetate	CC(C)COC(=O)C
RT-9.442		3-Carene	CC1 = CCC2C(C1)C2(C)C
RT-10.136		Sylvestrene	CC1 = CCC[C@H](C1)C(=C)C
RT-10.537		1-Hexanol, 2-ethyl-	CCCCCC(C)CO
RT-12.059		Imidazole	C1 = CN=CN1
RT-17.198		2,4-Imidazolidinedione, 3-methyl-	CN1C(=O)CNC1 = O
RT-23.895		Tromethamine	C(C(C)O)(CO)NO
RT-25.977		10-Methylnonadecane	CCCCCCCCC(C)CCCCCCCC
RT-27.353		Croctane	CC(C)CCCC(C)CCCC(C)CCCC(C)C
RT-32.041		3-Chloropropionic acid, heptadecyl ester	CCCCCCCCCCCCCCCCCOC(=O)CCCl
RT-33.247		1-Dodecanol, 2-hexyl-	CCCCCCCCC(CCCCC)CO
RT-33.782		Trichloroacetic acid, hexadecyl ester	CCCCCCCCCCCCCCCCCOC(=O)C(Cl)(Cl)Cl
RT-34.671		2-Isopropyl-5-methyl-1-heptanol	CCC(C)CCC(CO)C(C)C
RT-36.072		1,4-Benzenedicarboxylic acid, bis(2-ethylhexyl) ester	CCCCC(C)COC(=O)C1 = CC=C(C=C1)C(=O)OCC(C)CCCC
RT-40.224		Terephthalic acid, 3-hexyl octyl ester	CCCCCCCCCOC(=O)C1 = CC=C(C=C1)C(=O)OCC(C)CCC
RT-43.511		Ethanol, 2-(octadecyloxy)-	CCCCCCCCCCCCCCCCCOC
RT-41.661		Decanedioic acid, dibutyl ester	CCCCOC(=O)CCCCCCCCC(=O)OCCCC
RT-44.047		2-Methyl-Z-4-tetradecene	CCCCCCCC/C=C\C(C)C
RT-45.131		Heptacosyl pentafluoropropionate	CCCCCCCCCCCCCCCCCCCCCCCCCCCC(=O)C(C(F)(F)F)(F)F

respectively. (Tatiya et al., 2011). Murukan et al., (2018) reported that purified anthocyanin from *B. retusa* exhibited significant DPPH scavenging activity with an IC₅₀ of 0.31 mg/ml, ABTS+scavenging activity with an IC₅₀ of 0.55 mg/ml, and a high ferric-reducing capability (414.5 μmol Fe (II)/mg). Saneera et al., (2016) found that chloroform, hexane, and methanol extracts of *B. retusa* demonstrated notable DPPH and ABTS scavenging activities. The methanol extracts of leaves, stems, and fruits had IC₅₀ values of 0.52 ± 0.031 mg/mL, 0.12 ± 0.003 mg/mL, and 0.17 ± 0.005 mg/mL for DPPH, and 0.67 ± 0.007 mg/mL, 1.41 ± 0.001

mg/mL, and 5.58 ± 0.009 mg/mL for ABTS. Ogbonnia et al. (2021) noted that various solvent fractions of *Bridelia ferruginea* showed higher antioxidant activities compared to the crude extract.

Our finding is affirmative to previous findings by some authors. Still, the contribution of our study is GC-MS-based recognition of a wide spectrum of phytochemicals from *B. retusa* which strongly supports the therapeutic application of the plant by traditional healers worldwide.

Table 2
Drug-likeness properties of selected ligand molecules of *B. retusa*.

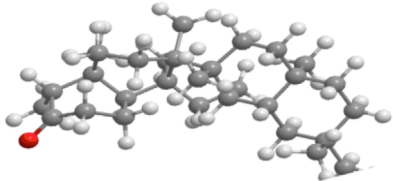
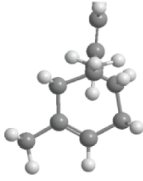
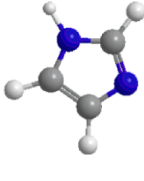
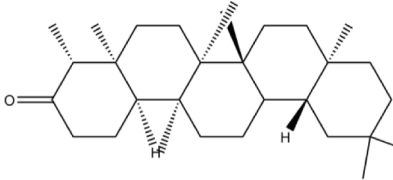
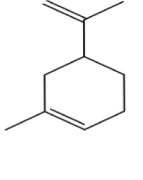
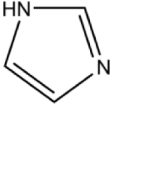
S. No.	Drug-likeness properties	Friedelin	Sylvestrene	Imidazole
	3D structure			
	2D structure			
	Molecular formula	C ₃₀ H ₅₀ O	C ₁₀ H ₁₆	C ₃ H ₄ N ₂
	Molecular weight	426.7	136.23	68.08
	LogP	9.8	3.4	-0.1
	H-bond Acceptor	1	0	1
	H-bond Donor	0	0	1
	Rotatable Bond	0	1	0
	Topological Polar Surface Area	17.1\AA ²	0\AA ²	28.7\AA ²
	Heavy atom	31	10	5

Table 3

Molecular docking results of DPP-IV (PDB code: 4A5S), α -amylase (PDB code: 5KEZ), and α -glucosidase (PDB code: 1UOK) with selected ligands of *B. retusa* based on docking score.

S. No.	Ligand name	PubChem ID	Docking	DPP-IV	α -amylase	α -glucosidase
1	Friedelin	91472	Score (kcal/mol) Interacting residues	−9.3 Lys71, Asn74, Ile76, Leu90, Asn92, Phe95, Asp96, Phe98, His100, Ser101, Ile102, Tyr105	−9.8 Gln63, Tyr151, Leu162, Thr163, Leu165, Lys200, His201, Glu233, Ile235, Asp300	−10.3 Gly141, Ala142, Ala143, Leu162, Phe163, Phe203, Ser222, Gly223, His224, Phe227, Met228, Pro257, Phe281, Met284, Asp285, Lys293, Asp329, Gln330, Glu387, Lys413
2	Imidazole	795	Score (kcal/mol) Interacting residues	−3.6 Glu347, Met348, Ser349, Val354, Gly355, Ile375	−2.7 Ala198, Ser199, Lys200, His201, Glu233, Val234	−3.3 Asp60, Tyr63, Phe163, Arg197, Asp199, Val200, Glu255, His328, Asp329, Arg415
3	Sylvestrene	12304570	Score (kcal/mol) Interacting residues	−6.4 Lys71, Ile76, Glu91, Phe95, Ile102, Tyr105, Ile114, Leu116, Asn75, Leu90, Asn92, Asn74	−5.7 Trp58, Trp59, Tyr62, Gln63, His101, Leu165, Asp197, His299, Asp300	−5.3 Ala143, Leu162, Phe163, Val200, Phe203, His224, Phe227, Met228, Pro257

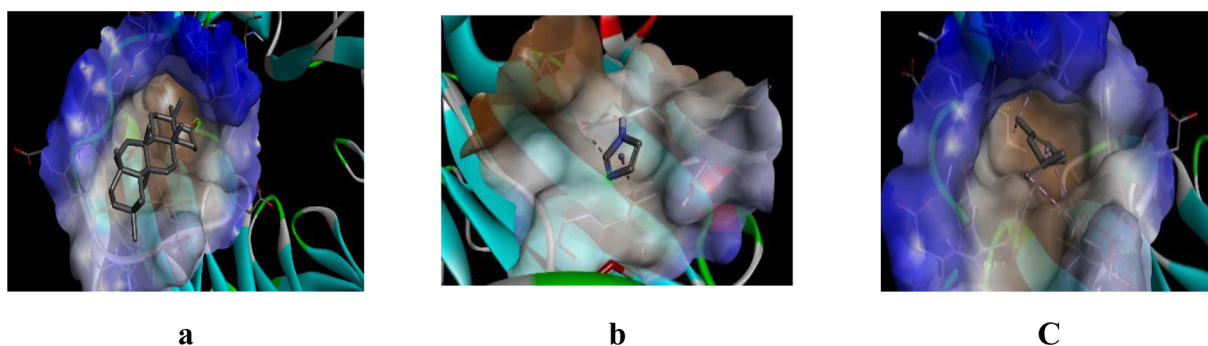


Fig. 3. 3D representation of best possible pose(s) of ligands- (a) friedelin, (b) imidazole, (c) sylvestrene within the active site of the target molecule (DPP-IV).

3.3. Antidiabetic activity

In the α -amylase inhibition assay, ethyl acetate bark extract showed the highest inhibition at 76.34 %. This was followed by methanolic fruit extract (74.05 % at 130.97 μ g/ml), ethyl acetate fruit extract (64.31 % at 153.36 μ g/ml), and methanolic bark extract (53.89 % at 181.7 μ g/ml) whereas, acarbose, the standard, achieved 84.07 % inhibition (99.52 μ g/ml). These results suggest the potential of *B. retusa* extract for anti-hyperglycemic activity, making it a candidate for managing hyperglycemia by inhibiting α -amylase, which can reduce post-meal blood glucose spikes (Lordan et al., 2013) (Fig. 1).

In the α -glucosidase enzyme inhibition assay we found a dose-dependent inhibition activity with standard drug acarbose. The methanolic fruit extract of *B. retusa* exhibited maximum α -glucosidase

inhibition activity with 86.18 % (106.15 μ g/ml), followed by the ethyl acetate fruit extract with 78.87 % (122.93 μ g/ml), ethyl acetate bark extract 77.04 % (124.01 μ g/ml) and methanolic bark extract 65.20 % (151.24 μ g/ml). While the standard drug acarbose revealed α -glucosidase inhibition of 88.96 % (89.85 μ g/ml) (Fig. 2).

Pancreatic α -amylase and α -glucosidase enzymes break down starches and sugars into monosaccharides, crucial for glucose absorption (Ochieng et al., 2017). Inhibiting α -glucosidase can delay glucose absorption and reduce postprandial hyperglycemia, as seen with medications like acarbose and voglibose (Matsui et al., 1996). Our study found that ethyl acetate bark extract and methanolic fruit extract of *B. retusa* effectively inhibited α -amylase and α -glucosidase, respectively, supporting its traditional use for diabetes management.

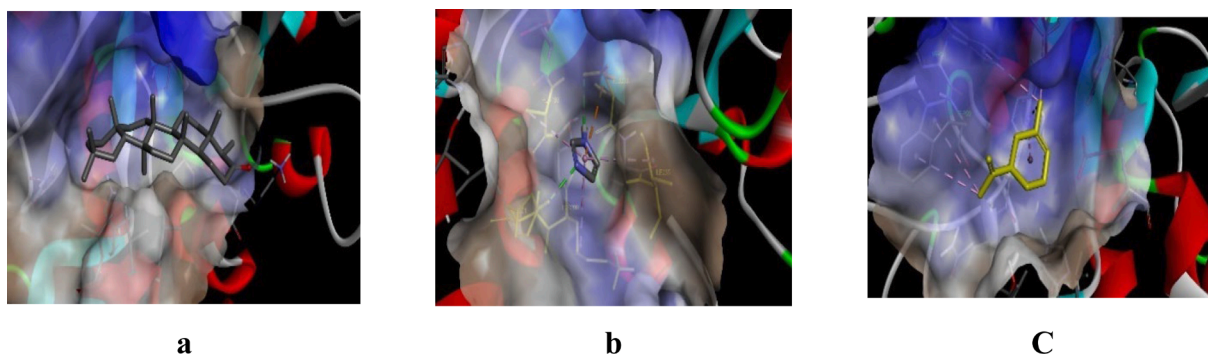


Fig. 4. 3D representation of best possible pose(s) of ligands- (a) friedelin, (b) imidazole, (c) sylvestrene within the active site of the target molecule (α -amylase).

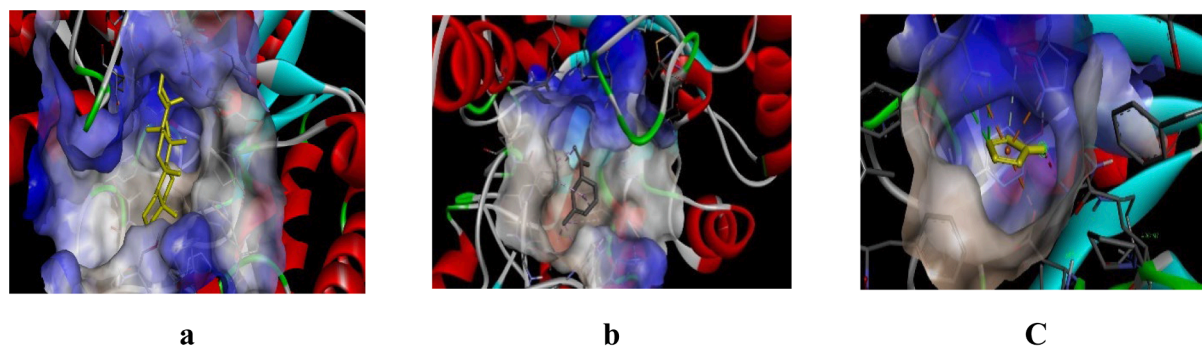


Fig. 5. 3D representation of best possible pose(s) of ligands- (a) friedelin, (b) imidazole, (c) sylvestrene within the active site of the target molecule (α -glucosidase).

3.4. Molecular docking

GC-MS analysis of *B. retusa* bark and fruit extracts identified 96 bioactive compounds (Table 1). For molecular docking, friedelin, imidazole, and sylvestrene were selected for interaction with three target proteins. Friedelin showed the most favorable binding with DPP-IV (-9.3 kcal/mol), α -amylase (-9.8 kcal/mol), and α -glucosidase (-10.3 kcal/mol), indicating superior binding affinity compared to imidazole and sylvestrene. Imidazole had the lowest affinity with binding energies of -3.6 kcal/mol, -2.7 kcal/mol, and -3.3 kcal/mol for DPP-IV, α -amylase, and α -glucosidase, respectively. Sylvestrene also showed better affinity than imidazole but less than friedelin (Table 2, 3; Figs. 3-5, Fig. S6-S8).

Friedelin interacted with 12 residues in DPP-IV (Lys71, Asn74, Ile76, Leu90, Asn92, Phe95, Asp96, Phe98, His100, Ser101, Ile102, Tyr105), 10 in α -amylase (Gln63, Tyr151, Leu162, Thr163, Leu165, Lys200, His201, Glu233, Ile235, Asp300), and 20 in α -glucosidase (Gly141, Ala142, Ala143, Leu162, Phe163, Phe203, Ser222, Gly223, His224, Phe227, Met228, Pro257, Phe281, Met284, Asp285, Lys293, Asp329, Gln330, Glu387, Lys413). Imidazole interacted with 6 residues in DPP-IV (Glu347, Met348, Ser349, Val354, Gly355, Ile375), 6 in α -amylase (Ala198, Ser199, Lys200, His201, Glu233, Val234), and 10 in α -glucosidase (Asp60, Tyr63, Phe163, Arg197, Asp199, Val200, Glu255, His328, Asp329, Arg415). Sylvestrene interacted with 12 residues in DPP-IV (Lys71, Ile76, Glu91, Phe95, Ile102, Tyr105, Ile114, Leu116, Asn75, Leu90, Asn92, Asn74), 9 in α -amylase (Trp58, Trp59, Tyr62, Gln63, His101, Leu165, Asp197, His299, Asp300), and 9 in α -glucosidase (Ala143, Leu162, Phe163, Val200, Phe203, His224, Phe227, Met228, Pro257).

Our investigation shows that the phytochemicals friedelin, imidazole, and sylvestrene from *B. retusa* significantly inhibit α -glucosidase, α -amylase, and DPP-IV. This suggests extract of *B. retusa* could aid in glucose control by slowing glucose release and improving blood sugar regulation. Molecular docking highlights friedelin as a promising candidate for developing new antidiabetic inhibitors targeting these enzymes.

Dipeptidyl peptidase IV (DPP-IV) inactivates glucagon-like peptide-1 (GLP-1) and glucose-dependent insulinotropic polypeptide (GIP), key incretin hormones. Inhibiting DPP-IV can help to regulate glucose levels in diabetes. α -Amylase, a calcium metalloenzyme, also contributes to elevated postprandial blood glucose and is a target for diabetes management (Kaur et al., 2021). Smruthi et al., (2016) found that phytochemicals from *Syzygium cumini* (e.g., friedelin, beta-sitosterol) interact with α -amylase with lower binding energies than acarbose. Similarly, compounds from other plants (e.g., 6 urs-12-en-24-oic acid from *P. zeylanica*) showed strong binding with DPP-IV and α -amylase, suggesting high potential for managing diabetes (Thamaraiselvi et al., 2021).

For α -glucosidase and α -amylase, compounds like acarbose and epigallocatechin gallate showed varying inhibitory activities, with

epigallocatechin gallate as notable (Oboh et al., 2014; Tadera et al., 2006). Docking of amentoflavone, friedelin, and 6-deoxyjacareubin with porcine pancreatic elastase yielded binding energies of -10.94 , -7.17 , and -6.72 kcal/mol, respectively, with friedelin showing strong interactions, including a Pi-sigma bond with His57 (Ambarwati et al., 2022). Muralikrishna et al. (2019) found that beta-sitosterol and friedelin from *Ficus racemose* had favorable interactions with hyperglycemic targets, with friedelin forming hydrogen bonds with Lys776. Drug-likeness properties of *B. retusa* compounds were assessed using SwissADME based on Lipinski's rule of five (Daina and Zoete, 2016).

Sylvestrene and imidazole met all Lipinski criteria viz. molecular weight (≤ 500), hydrogen bond acceptors (≤ 10), donors (≤ 5), and LogP (< 5). However, friedelin exceeded the LogP threshold, indicating high lipophilicity and potential issues with absorption (Bahmani et al., 2017). Despite this, all compounds showed favorable molecular weight and TPSA values, suggesting good absorption and permeability. Friedelin, along with sylvestrene and imidazole, exhibited promising antioxidant and antidiabetic activities, with friedelin standing out as the most effective candidate for diabetes therapy.

3.5. Molecular docking simulation analysis

MD simulations provide insights into protein-ligand interactions and ligand stability. We analyzed nine complexes: DPP-IV-Sylvestrene, DPP-IV-Imidazole, DPP-IV-Friedelin, α -amylase-Sylvestrene, α -amylase-Imidazole, α -amylase-Friedelin, α -glucosidase-Sylvestrene, α -glucosidase-Imidazole, and α -glucosidase-Friedelin (Fig. S9-S11). For stability assessment, RMSD and RMSF were monitored. RMSD analysis (Fig. S9a-c) showed that DPP-IV-Sylvestrene had the most stable RMSD (0.2–0.3 nm), while DPP-IV-Imidazole and DPP-IV-Friedelin had higher deviations. The α -amylase-Friedelin complex was the most stable (0.15–0.25 nm) compared to the other α -amylase complexes. For α -glucosidase, α -glucosidase-Friedelin was the most stable, with RMSD values of 0.15–0.35 nm initially, decreasing to 0.27–0.33 nm later. Higher RMSF values were observed for the imidazole complex, indicating greater fluctuation compared to sylvestrene and friedelin (Fig. S9d-f).

Radius of gyration (Rg) analysis measures the compactness of protein-ligand complexes, reflecting structural stability and integrity. Elevated Rg values suggest decreased compactness and potential structural instability, while lower values indicate a more stable structure. For DPP-IV protein complexes, Rg values ranged from 2.7 to 2.8 nm for all three drugs (Fig. S10a). For α -amylase, Rg values were between 2.32 and 2.4 nm for all drugs (Fig. S10b). For α -glucosidase, Rg values ranged from 2.42 to 2.57 nm, with the α -glucosidase-Friedelin complex showing the lowest Rg values of 2.43 to 2.47 nm (Fig. S10c).

Intermolecular hydrogen bond (H-Bond) analysis was performed for DPP-IV, α -amylase, and α -glucosidase with sylvestrene, imidazole, and friedelin. For DPP-IV, imidazole formed a maximum of 2 hydrogen bonds during 40–50 ns and 80–90 ns, while friedelin formed 1 hydrogen

Table 4

MM-PBSA analysis for final target proteins (DPP-IV, α -amylase, and α -glucosidase) complexed with final drugs sylvestrene, imidazole and friedelin.

Protein-Ligand Complex	Van der Waal Energy (kJ/mol)	Electrostatic Energy (kJ/mol)	Polar Solvation Energy (kJ/mol)	Binding Energy (kJ/mol)
DPP-IV-Sylvestrene	-100.509 +/- 6.778	-0.850 +/- 3.256	51.910 +/- 8.641	-60.457 +/- 11.215
DPP-IV-Imidazole	-60.457 +/- 11.215	-60.457 +/- 11.215	12.816 +/- 97.276	11.732 +/- 96.795
DPP-IV-Friedelin	-66.763 +/- 60.857	-16.233 +/- 21.324	41.508 +/- 89.146	-49.45 +/- 54.854
α -amylase-Sylvestrene	-33.493 +/- 18.505	-0.515 +/- 1.936	18.155 +/- 19.946	-21.229 +/- 28.937
α -amylase-Imidazole	-1.402 +/- 4.102	-0.305 +/- 3.357	-1.773 +/- 36.396	-3.694 +/- 36.136
α -amylase-Friedelin	-140.119 +/- 10.377	-0.521 +/- 1.631	42.387 +/- 5.526	-114.467 +/- 8.982
α -glucosidase-Sylvestrene	-62.842 +/- 8.486	-1.176 +/- 2.106	24.748 +/- 15.303	-48.116 +/- 16.377
α -glucosidase-Imidazole	-4.738 +/- 6.795	-3.351 +/- 12.650	20.483 +/- 73.965	11.342 +/- 74.759
α -glucosidase-Friedelin	-148.948 +/- 10.475	3.879 +/- 4.881	60.083 +/- 15.311	-102.904 +/- 15.329

bond from 1 to 93 ns but none later, and sylvestrene formed no hydrogen bonds (Fig. S10d). For α -amylase, no hydrogen bonds were observed with sylvestrene, and friedelin formed a few single bonds around 20–30 ns and 45 ns. The α -amylase-imidazole complex formed 3 hydrogen bonds initially and exhibited intermittent bonding throughout the simulation (Fig. S10e). For α -glucosidase, sylvestrene formed no hydrogen bonds. Friedelin and imidazole formed 1–3 hydrogen bonds intermittently during the simulation (Fig. S10e).

SASA analysis was performed to evaluate the protein surface area exposed to water, indicating the extent of drug interaction. For DPP-IV, SASA values ranged from 320 to 350 nm² (Fig. S11a). For α -amylase, SASA values were lower, between 185 to 225 nm² (Fig. S11b), suggesting a stronger drug interaction. For α -glucosidase, SASA values

ranged from 230 to 270 nm² (Fig. S11c). The lower SASA values for α -amylase indicate a more stable drug interaction due to reduced protein surface exposure to water.

PCA analysis was used to assess protein–ligand complex stability by examining eigenvector variances. For DPP-IV, the sylvestrene complex had the least variance, with eigenvector values ranging from -3 to 3 nm (Fig. S11d), compared to -20 to 20 nm for imidazole and -60 to 40 nm for friedelin. For α -amylase, eigenvector values were -27 to 15 nm (sylvestrene), -16 to 18 nm (imidazole), and -10 to 6 nm (friedelin) (Fig. S11e), with the α -amylase-friedelin complex showing the least conformational changes. For α -glucosidase, eigenvector values ranged from -27 to 30 nm (sylvestrene), -18 to 17 nm (imidazole), and -4 to 4 nm (friedelin) (Fig. S11f). The best PCA values were observed for the α -glucosidase-friedelin complex, followed by α -amylase-friedelin and DPP-IV-sylvestrene complexes.

3.6. Binding free energy calculations of top drugs complexed with anti-diabetic target proteins

MM-PBSA free energy calculations were performed on the complexes of sylvestrene, imidazole, and friedelin with DPP-IV, α -amylase, and α -glucosidase, using MD trajectories from the last 10 ns (90–100 ns). The analysis highlighted van der Waals, electrostatic, and polar solvation energies as key stabilizers (Table 4). The maximum ΔG_{Bind} values were -60.457 ± 11.215 kJ/mol for DPP-IV-sylvestrene, -114.467 ± 8.982 kJ/mol for α -amylase-friedelin, and -102.904 ± 15.329 kJ/mol for α -glucosidase-friedelin. Among these, the α -amylase-friedelin complex exhibited the highest ΔG_{Bind} .

Molecular dynamics simulations revealed stability and structural dynamics in nine protein–ligand complexes. Friedelin showed the most stable interactions with DPP-IV, α -amylase, and α -glucosidase, indicated by lower RMSD and RMSF values. SASA analysis highlighted strong interactions, particularly with α -amylase. PCA revealed distinct conformational changes for each complex. MM-PBSA calculations highlighted van der Waals, electrostatic, and polar solvation energies as key stabilizers, with the α -amylase-friedelin complex showing the

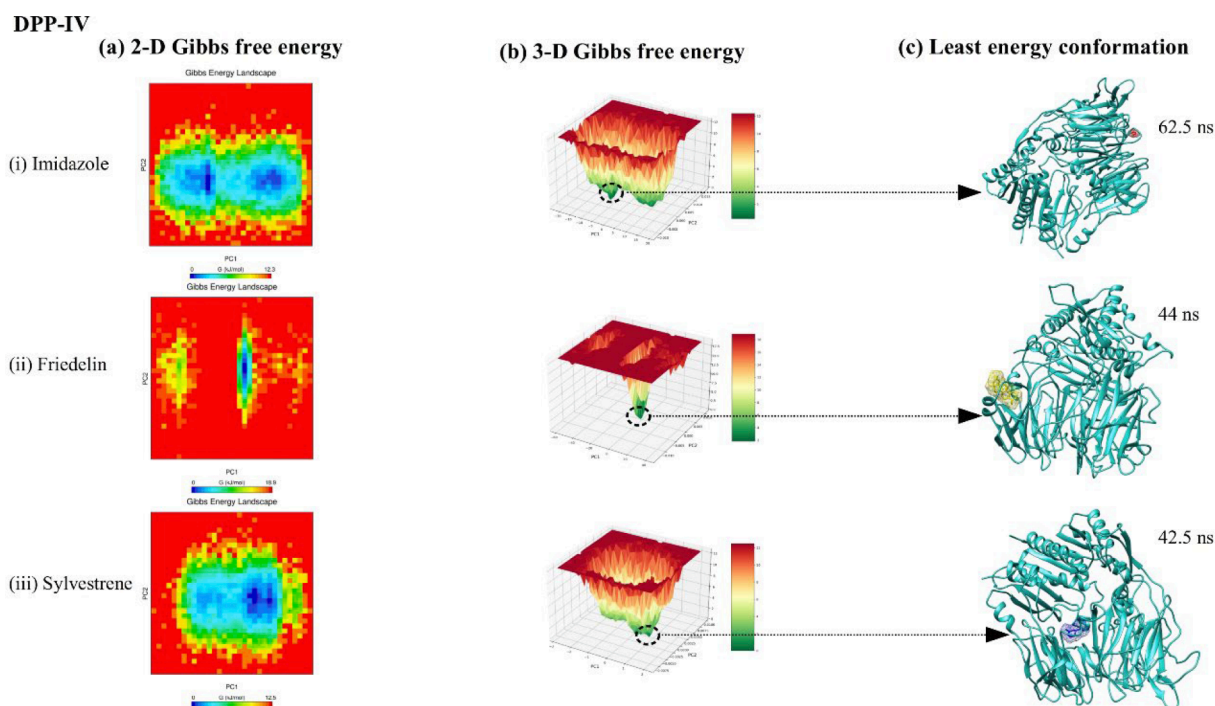


Fig. 6. showing 2-D, 3-D principal component analysis along with free energy landscape plot for DPP-IV protein complexed with ligands imidazole, friedelin, and sylvestrene.

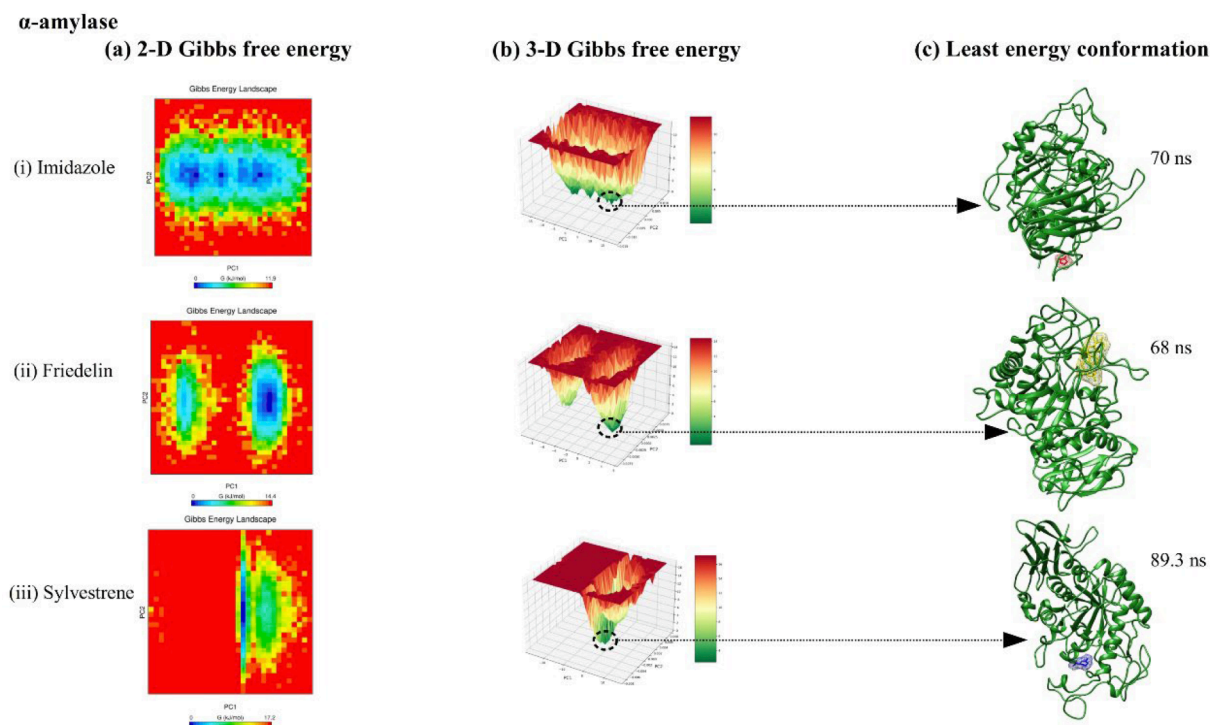


Fig. 7. showing 2-D, 3-D principal component analysis along with free energy landscape plot for alpha-amylase protein complexed with ligands imidazole, friedelin, and sylvestrene.

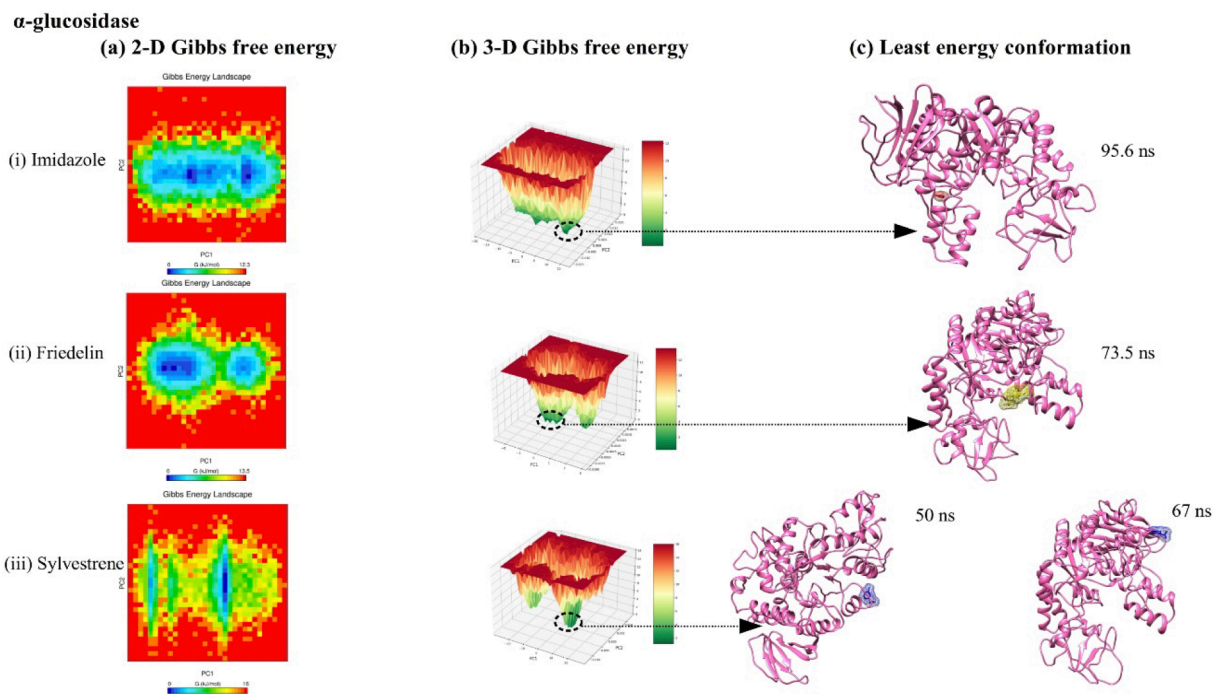


Fig. 8. showing 2-D, 3-D principal component analysis along with free energy landscape plot for alpha-glucosidase protein complexed with ligands imidazole, friedelin, and sylvestrene.

highest binding energy.

Free energy landscape (FEL) analysis for DPP-IV, α -amylase, and α -glucosidase complexes with imidazole, friedelin, and sylvestrene is shown in Figs. 6, 7, and 8. The 2D FEL plots (Fig. 6(a–b), 7(a–b), 8(a–b)) use red for maximum Gibbs free energy and blue for minimum Gibbs free energy, while the 3D FEL plots use red and dark green similarly. For DPP-IV, the least energy conformations occurred at 62.5 ns (imidazole),

44 ns (friedelin), and 42.5 ns (sylvestrene) (Fig. 6(c)). For α -amylase, they were at 70 ns (sylvestrene), 68 ns (imidazole), and 89.3 ns (friedelin) (Fig. 7(c)). For α -glucosidase, the least energy conformations were at 95.6 ns (imidazole), 73.5 ns (friedelin), and at 50 ns and 67 ns (sylvestrene) (Fig. 8(c)).

4. Conclusion

Diabetes remains a global challenge, with many relying on insulin. The scientific community seeks effective compounds to inhibit key regulatory receptors for diabetes control. We investigated *B. retusa* and identified promising compounds- sylvestrene, imidazole, and friedelin-known for their antioxidant properties and inhibition of α -amylase and α -glucosidase in *in vitro*. Molecular docking and drug-likeness studies support their potential. Based on antioxidant activity and *in silico* studies, we recommend Friedelin as the most promising candidate for drug development against diabetes.

Funding

The present study was supported by CSIR-India (Id: 08/526(0003)/2019-EMR-I) for Fellowship, and King Saud University under Researcher Supporting Project [RSPD2024R712].

CRediT authorship contribution statement

Somendra Kumar: Investigation. **Dinesh Kumar:** Validation. **Motiram Sahu:** Writing – original draft. **Neha Shree Maurya:** Data curation. **Ashutosh Mani:** Writing – review & editing. **Chandramohan Govindasamy:** Conceptualization. **Anil Kumar:** Supervision, Conceptualization.

Declaration of competing interest

The authors declare that they have no known competing financial interests or personal relationships that could have appeared to influence the work reported in this paper.

Acknowledgement

The present study was supported by CSIR-India (Id.08/526(0003)/2019-EMR-1) for Fellowship, and also, this project was supported by Researchers Supporting Project number (RSPD2024R712), King Saud University, Riyadh, Saudi Arabia.

Appendix A. Supplementary material

Supplementary material to this article can be found online at <https://doi.org/10.1016/j.jksus.2024.103411>.

References

- Adhav, M., Solanki, C.M., Patel, B., Ghorla, A., 2002. Evaluation of isoflavanone as an antimicrobial agent from leaves of *Bridelia retusa* (L.). *Orient. J. Chem.* 18, 476–479.
- Ambarwati, N.S.S., Azminah, A., Ahmad, I., 2022. Molecular docking, physicochemical and drug-likeness properties of isolated compounds from *Garcinia latissima* Miq. on elastase enzyme: In silico analysis. *Pharma. J.* 14 (2), 282–288.
- Bahmani, A., Saaipour, S., Rostami, A., 2017. A simple, robust, and efficient computational method for n-octanol/water partition coefficients of substituted aromatic drugs. *Sci. Rep.* 7 (1), 1–12.
- Daina, A., Zoete, V., 2016. A BOILED-Egg to predict gastrointestinal absorption and brain penetration of small molecules. *ChemMedChem* 11, 1117–1121.
- Eom, S.H., et al., 2012. α -Glucosidase and α -amylase-inhibitory activities of phlorotannins from *Eisenia bicyclis*. *J. Sci. Food Agric.* 92, 2084–2090.
- Ghawate, V.B., Bhambar, R.S., Bairagi, S.M., Jadhav, V.S., 2014. Hepatoprotective activity of *Bridelia retusa* against paracetamol-induced liver damage in Swiss albino mice. *Asian J. Biol. Sci.* 7, 217–224.
- Hess, B., Bekker, H., Berendsen, H.J., Fraaije, J.G., 1997. LINC: A linear constraint solver for molecular simulations. *J. Comput. Chem.* 18 (12), 1463–1472.
- Huang, J., MacKerell Jr., A.D., 2013. CHARMM36 all-atom additive protein force field: Validation based on comparison to NMR data. *J. Comput. Chem.* 34 (25), 2135–2145.
- Jayasinghe, B.M.M., Kumarihamy, K.H.R.N., Jayarathna, N.W.M.G., Udishani, B.M.R., Bandara, N., Hara, Y., Fujimoto, Y., 2003. Antifungal constituent of the stem bark of *Bridelia retusa*. *Phytochemistry* 62, 637–641.

- Karamian, R., Azizi, A., Asadbegy, M., Pakzad, R., 2014. Essential oil composition and antioxidant activity of the methanol extracts of three *Phlomis* species from Iran. *J. Biol. Active Products Nat.* 4 (5–6), 343–353.
- Kaur, N., Kumar, V., Nayak, S.K., Wadhwa, P., Kaur, P., Sahu, S.K., 2021. Alpha-amylase as a molecular target for the treatment of diabetes mellitus: A comprehensive review. *Chem. Biol. Drug Des.* 98 (4), 539–560.
- Konappa, N., Udayashankar, A.C., Krishnamurthy, S., Pradeep, C.K., Chowdappa, S., Jogaiah, S., 2020. GC-MS analysis of phytoconstituents from *Amomum nilgircicum* and molecular docking interactions of bioactive serovergenin acetate with target proteins. *Sci. Rep.* 10 (1), 16438.
- Kumar, T., Jain, V., 2014. Antinociceptive and anti-inflammatory activities of *Bridelia retusa* methanolic fruit extract in experimental animals. *Scient. World J.* 2014, 890151.
- Kurjogi, M., Satapute, P., Jogaiah, S., Abdelrahman, M., Daddam, J.R., Ramu, V., Tran, L. P., 2018. Computational modeling of the staphylococcal enterotoxins and their interaction with natural antitoxin compounds. *Int. J. Mol. Sci.* 19 (1), 133.
- Lee, K., Kim, D., 2019. *In-silico* molecular binding prediction for human drug targets using deep neural multi-task learning. *Genes* 10, 906.
- Lordan, S., Smyth, T.J., Soler-Vila, A., Stanton, C., Ross, R.P., 2013. The α -amylase and α -glucosidase inhibitory effects of Irish seaweed extracts. *Food Chem.* 141 (3), 2170–2176.
- Loza-Mejía, M.A., Salazar, J.R., Sánchez-Tejeda, J.F., 2018. In silico studies on compounds derived from *Calceolaria*: phenylethanoid glycosides as potential multitarget inhibitors for the development of pesticides. *Biomolecules* 8, 121.
- Mallard, W.G., Linstrom, P.J., 2008. NIST Standard Reference Database. National Institute of Standards and Technology.
- Matsui, T., Yoshimoto, C., Osajima, K., Oki, T., Osajima, Y., 1996. In vitro survey of alpha-glucosidase inhibitory food components. *Biosci. Biotech. Bioch.* 60 (12), 2019–2022.
- Muralikrishna, P., Duraiswamy, B., Nair, N.K., 2019. In silico docking and in vitro enzyme inhibition activity of unripe fruits of *Ficus racemosa* Linn. *Eur. J. Pharm. Med. Res.* 5 (6).
- Murukan, G., Kavitha, C.H., Lawrence, B., Aswathy, J.M., Murugan, K., 2018. Purified anthocyanin from *Bridelia retusa* (L.) Spreng. as antioxidant and antimicrobial: A medicinal plant from South Western Ghats, Kerala. *Int. J. Pharm. Res. Health Sci.* 6, 2250–2257.
- Ngueym, T.A., Brusotti, G., Caccialanza, G., Finzi, P.V., 2009. The genus *Bridelia*: A phytochemical and ethnopharmacological review. *J. Ethnopharmacol.* 124, 339–349.
- Oboh, G., Ademosun, A.O., Ayeni, P.O., 2014. Comparative effect of quercetin and rutin on α -amylase, α -glucosidase, and some pro-oxidant-induced lipid peroxidation in rat pancreas. *Comp. Clin. Pathol.* 24, 1103–1110.
- Ochieng, P., Sumaryada, T., Okun, D., 2017. Molecular docking and pharmacokinetic prediction of herbal derivatives as a maltase-glucoamylase inhibitor. *Asian J. Pharm. Clin. Res.* 10, 392.
- Ogbonnia, S.O., Ginikachukwu, O., Ezemenahi, S.I., Okeke, A.I., Ota, D., 2021. Preliminary phytochemistry, antioxidant activities, and GC/MS of the most abundant compounds of different solvent fractions of the plant *Bridelia ferruginea* Benth used locally in the management of diabetes. *J. Pharma. Phytochem.* 10 (3), 154–164.
- Rupali, B.D., Narayan, N.P., Yuvraj, D.A., 2016. An overview of *Bridelia retusa* Linn. *World J. Pharm. Res.* 4, 199–203.
- Sanseera, D., Liawruangrath, B., Pyne, S.G., Liawruangrath, S., 2016. Determination of antioxidant and anticancer activities together with total phenol and flavonoid contents of *Cleidion javanicum* Bl. and *Bridelia retusa* (L.) A. Juss. *Chiang Mai J. Sci.* 43, 534–545.
- Smruthi, G., Mahadevan, V., Vadivel, V., Brindha, P., 2016. Docking studies on antidiabetic molecular targets of phytochemical compounds of *Syzygium cumini* (L.) Skeels. *Asian J. Pharm. Clin. Res.* 9 (9), 287–293.
- Tadera, K., Minami, Y., Takamatsu, K., Matsuoka, T., 2006. Inhibition of alpha-glucosidase and alpha-amylase by flavonoids. *J. Nutr. Sci. Vitaminol. (tokyo)* 52 (2), 149–153.
- Tatiya, A., Saluja, A., Kalaskar, M., Surana, S., Patil, P., 2017. Phytochemical characterization and anti-inflammatory activity of *Bridelia retusa* bark Spreng. in acute and chronic inflammatory conditions: A possible mechanism of action. *EJPMR* 4, 686–696.
- Tatiya, A.U., Tapadiya, G.G., Kotecha, S., Surana, S.J., 2011. Effect of solvents on total phenolics, antioxidant and antimicrobial properties of *Bridelia retusa* Spreng. stem bark. *IJNPR* 2, 442–447.
- Thamaraiselvi, L., Selvankumar, T., Wesely, E.G., Nathan, V.K., 2021. In silico molecular docking on bioactive compounds from Indian medicinal plants against type 2 diabetic target proteins: A computational approach. *Indian J. Pharm. Sci.* 83 (6), 1273–1279.
- Umar, A.K., Zothantluanga, J.H., Aswin, K., Maulana, S., Sulaiman Zubair, M., Lalthlenmawia, H., Rudrapal, M., Chetia, D., 2022. Antiviral phytochemicals “ellagic acid” and “(+)-sesamin” of *Bridelia retusa* identified as potential inhibitors of SARS-CoV-2 3CLpro using extensive molecular docking, molecular dynamics simulation studies, binding free energy calculations, and bioactivity prediction. *Struct. Chem.* 1–21.
- Van Der Spoel, D., Lindahl, E., Hess, B., Groenhof, G., Mark, A.E., Berendsen, H.J., 2005. GROMACS: Fast, flexible, and free. *J. Comput. Chem.* 26 (16), 1701–1718.
- Vanommelaeghe, K., Hatcher, E., Acharya, C., Kundu, S., Zhong, S., Shim, J., Darian, E., Guvench, O., Lopes, P., Vorobyov, I., MacKerell Jr., A.D., 2010. CHARMM General Force Field: A force field for drug-like molecules compatible with the CHARMM all-atom additive biological force field. *J. Comput. Chem.* 31, 671–690.